

Supporting Information for

Viscoelastic relaxation of cellulose nanocrystals in fluids: Contributions of microscopic internal motions to flexibility

Reina Tanaka^{,†,‡} Yu Kashiwagi,[†] Yuki Okada,[†] and Tadashi Inoue[†]*

[†] Department of Macromolecular Science, Graduate School of Science, Osaka University,
1-1 Machikaneyama-cho, Toyonaka, Osaka 560-0043, Japan

[‡] Forestry and Forest Products Research Institute, Forest Research and Management
Organization, 1 Matsunosato, Tsukuba, Ibaraki 305-8687, Japan

Email: tanakar1101@ffpri.affrc.go.jp

S1. Concentration dependence of viscoelastic functions and critical concentration of the CNC/glycerol dispersions.

Molecular theories, such as the Morse theory, used in this study are derived assuming infinite dilution. Therefore, the experimental results obtained at finite concentrations are normally extrapolated to infinite dilution, and the intrinsic modulus $[G^*] \equiv \lim_{c \rightarrow 0} \frac{G^*}{c}$ is calculated to compare with the theoretical predictions. However, a dilute dispersion of CNC can be achieved at very low concentrations, and therefore the extrapolation to infinite dilution was found not to be so accurate. Results at finite concentrations, G^*/c may be slightly different from those at infinite dilution, $[G^*]$. Here, we discuss the experimental error arising from using G^* as $[G^*]c$. The threshold to distinguish dilute solutions and semi-dilute solutions is the overlap critical number density, ν^* , or the critical concentration, c^* , and these values for rod like polymers can be estimated as

$$v^* = L^{-3} \quad (S1)$$

In the case of CNCs, c^* can be described as

$$c^* = \rho V_c L^{-3} \quad (S2)$$

Here, V_c is the volume of the CNCs ($=L_w W_w h$) and ρ is the density of the CNCs (1.63 g cm⁻³). Thus, the estimated c^* is tabulated in Table S1. In the case of C-CNC and S-CNC, the sample concentration is lower than c^* , while in the case of T-CNC, the sample concentration is slightly higher than c^* . Here we note that c^* is a general measure and not a universal value for all physical properties. The actual threshold concentration can vary with physical properties.

The concentration dependence of viscoelastic functions can be characterized with the intrinsic viscosity, $[\eta] \equiv \lim_{c \rightarrow 0} \frac{\eta - \eta_s}{\eta_s c}$. For example, the concentration dependence of viscosity can be described as

$$\frac{\eta - \eta_s}{\eta_s c} = [\eta] \{1 + k_H [\eta] c + \dots\} \quad (S3)$$

Here, k_H is Huggins' coefficient and experimentally determined as ≤ 0.5 for rigid and semiflexible polymers.¹⁻² Equation S3 indicates that in the case of $[\eta]c < 1$, $\frac{\eta - \eta_s}{\eta_s c}$ can be used as $[\eta]$ in the first approximation, and also that the experimental error arising from regarding $\frac{\eta - \eta_s}{\eta_s c}$ at finite concentrations as $[\eta]$ can be estimated as $k_H [\eta] c$. The

molecular origin of the difference between $\frac{\eta-\eta_s}{\eta_s c}$ at finite concentrations and $[\eta]$ is attributed to the slowdown of the rotational motion of polymer by the molecular interactions. Therefore, a similar discussion is applicable to $[G^*]$.

We estimated the $[\eta]$ values for CNCs using an equation for rotational motions of rod-like polymers in the dilute region.³

$$[\eta] = \frac{2\pi L_w^3}{45 (\ln(p)-0.8) \rho V_C} \frac{1}{c} \quad (\text{S4})$$

The obtained values of $[\eta]$ and $[\eta]c$ are listed in Table S1. Thus, the difference between G^*/c and $[G^*]$ can be characterized with $k_H[\eta]c$, which is estimated to be less than 5% for $k_H \sim 0.5$. These results indicate that the CNC/glycerol dispersions at the examined solid concentrations c were sufficiently dilute, and thus the molecular theories developed for infinite dilute system were applicable to our CNC/glycerol dispersions.

Table S1. Summary of the examined weight percentage concentration w , weight concentration per unit volume c , intrinsic viscosity $[\eta]$, the product of $[\eta]$ and c , and the critical concentration c^* .

	C-CNC	S-CNC	T-CNC
$w / \% \text{ w/w}$	0.15	0.010	0.030
c / gcm^{-3}	0.00189	0.00013	0.00038
$[\eta] / \text{cm}^3\text{g}^{-1}$	17	80	228
$[\eta]c$	0.032	0.010	0.086
c^* / gcm^{-3}	0.00362	0.00054	0.00016

S2. Theoretical background

Here we briefly explain the molecular theory for semiflexible polymers which is applied to the CNC dispersions in this study. Conformation of polymer chains may be characterized with the wormlike chain model. In this model, important parameters are the chain contour length, L , and the persistent length, $L_p \equiv \kappa/k_B T$, which is defined as the ratio of the chain bending rigidity κ to the thermal energy $k_B T$. In the case of semiflexible polymers of $L/L_p \leq 1$, the conformation of the polymers is not straight and the polymers undergo the thermally-excited transverse undulations due to the small bending motions.⁴ Thus, their end-to-end lengths are always shorter than L values. As a result, effective extensibility occurs and produces internal motions, or tension and bending. The tension mode arises from constraint forces which restrict to extend semiflexible rods in the longitudinal direction. Thus, thermally undulated structure of the polymer originates the tension along the chain in addition to the bending stress, and these stresses contribute the relaxation modulus. According to Shankar et al., the intrinsic complex modulus, $[G^*] \equiv \lim_{c \rightarrow 0} \frac{G^* - i\eta_s}{c}$, for semiflexible polymers of $L/L_p \leq 1$ can be described as follows.⁴

$$[G^*] = [G_{ort}^*] + [G_{curve}^*] + [G_{tens}^*] \quad (S5)$$

The $[G_{ort}^*]$ represents the modulus originated by the entropic stress due to the orientation of the end-to-end vector of the polymer. The $[G_{curve}^*]$ and $[G_{tens}^*]$ respectively represent the contribution of the bending stress and the tension stress. Corresponding molecular motions are explained with Figure S1. The theory provides the functional form of these three components of modulus, and we used in section 4 in Results

and Discussion. The validity of the theory was examined with the experimental results of poly (γ -benzyl-*L*-glutamate) (PBLG) solutions. We note $[G_{tens}^*]$ significantly contributes to the modulus, even in the case of almost rigid rods with $\frac{L}{L_p} = 0.01$, as shown in Figure 9.

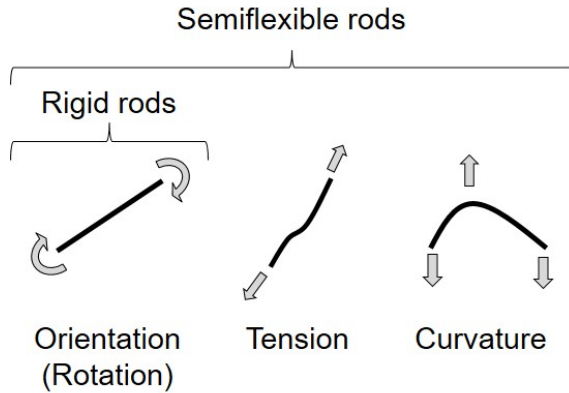


Figure S1. Schematic illustration of orientational (rotational) and internal (tension and curvature) motions. In the case of rigid rods, stress is originated solely from orientation of rods. In the case of semiflexible rods, stress is originated from the combination of the orientational and the internal motions.

The strain-induced birefringence, Δn , mainly reflects the orientation of the chain.⁵ This is simply because the conformation change due to the thermally undulated structure is much smaller than the orientation. Thus, the complex strain-optical coefficient K^* , which is the complex ratio of the shear component of the refractive index tensor n_{xy} to oscillatory strain,⁶ can be written as follows.

$$[K^*] = [K_{ort}^*] = C_{SO}(L)[G_{ort}^*] \quad (S6)$$

Here, $C_{SO}(L)$ is the stress-optical coefficient and can be related to the optical anisotropy of unit length of structure units, $\Delta\alpha$. In the case of $L/L_P < 1$, $C_{SO}(L)$ is given as $\frac{2\pi(n^2+2)^2\Delta\alpha L}{45nk_B T} = CL$.⁶ In the concentrated regime, the structural birefringence due to the regular distribution of rods or orientational ordering may be observed, and such birefringence can be ignored in the dilute regime where we employed the experiments.

To obtain $[G^*]$ (or $[K^*]$), normally G^* is measured as a function of concentration c in the dilute regime and extrapolated to $c \rightarrow 0$. However, the dilute regime of the CNC dispersions is quite low (C-CNC: $< 0.00362 \text{ gcm}^{-3}$, S-CNC: $< 0.00054 \text{ gcm}^{-3}$, T-CNC: $< 0.00016 \text{ gcm}^{-3}$) as discussed in Supporting information S1, and the accurate concentration extrapolation could not be achieved, due to the limitation of sensitivity of our apparatus. Therefore, we applied the theory with the first approximation.

$$G^* = c[G^*] + i\omega\eta_s \quad (S7)$$

where η_s is the dispersion medium viscosity.

Experimental error due to this approximation is estimated to be less than 5% as discussed in Supporting information S1. Similar approximations for dilute solutions are widely used in the molar mass estimation by the light scattering apparatus combined with the size exclusion chromatography. The same approximation is applied to the birefringence data.

S3. Small-angle X-ray scattering (SAXS) measurements of the CNCs in glycerol

SAXS measurements were performed on T-CNC dispersed in water or glycerol using a SAXSpase (Anton Paar GmbH.), and data processing was carried out using the SAXSanalysis program. The T-CNC/glycerol dispersion was added to the quartz liquid

cells of a TCStage 150 sample holder unit. A high-flux sealed-tube X-ray beam in line collimation (Cu K α radiation, $\lambda = 0.1542$ nm) was used, and scattered intensities were recorded during the exposure time of 15 min on a 1D hybrid photon counting detector (Mythen). The sample to detector distance was set as 317 mm. The scattering intensity recorded from glycerol was used for the background subtraction to each scattering curve (Figure S2a). Indirect Fourier transformation (IFT) fitting was conducted on the background-subtracted intensity curves under the assumption that the shape of T-CNC was a significantly long rod with a rectangular cross-section.⁷ 2D pair-distance distribution $P_c(r)$ functions for the cross-section of T-CNC were then calculated as a function of dimension. A T-CNC/water dispersion was used as a reference sample. A similar experiment was also conducted on the T-CNC/water dispersion.

Figure S2a shows background-subtracted scattering curves of the T-CNC/glycerol and T-CNC/water dispersions. Although the intensities for the T-CNC/water dispersion were slightly higher than those for the T-CNC/glycerol dispersion depending on the electron density difference between the dispersion medium and T-CNC, the shape of the scattering curves was similar. A model-independent collimation correction (desmearing) process was conducted on the background-subtracted scattering curves by the Lake algorithm.⁸ The desmeared data were compared with the IFT fitted curves (Figure S2b). The desmeared data were overlapped with the IFT-fitted curves. These results showed that the IFT fitting was conducted well on the background-subtracted scattering curves, and the assumption that T-CNC is a long rod was reasonable. Figure S2c shows the $P_c(r)$ functions of the T-CNC/water and T-CNC/glycerol dispersions as a function of dimension. The $P_c(r)$ functions of both the T-CNC dispersions showed similar tendency regardless of dispersion medium; the functions became convex upward at ~ 5 nm, and asymptotic to

zero at 23–24 nm. A shoulder-like small bump in $P_c(r)$ of T-CNC/water around 20 nm (black line in Fig. S2c) indicated the existence of a small amount of components with larger cross-sections. However, the maximum dimensions in the cross-section of T-CNC (23–24 nm) were almost the same regardless of dispersion medium (water or glycerol). These results show that T-CNC in glycerol had similar dimensions in cross-section to that in water. Namely, CNCs were dispersed in glycerol without aggregation, as in water.

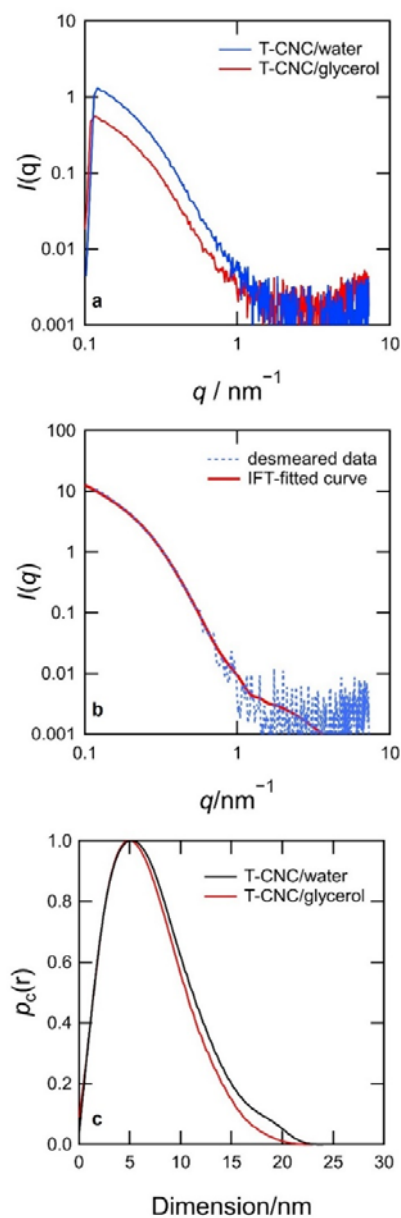


Figure S2. (a) Background-subtracted scattering curves of the T-CNC/glycerol and T-CNC/water dispersions (b) Comparison of the desmeared data by Lake algorithm (blue dashed line) for the T-CNC/glycerol dispersion with the IFT-fitted curve (red solid line). (c) $P_c(r)$ functions obtained by IFT fitting for the cross section of the T-CNC in glycerol and water.

S4. Length distribution functions determined from the birefringence data

The length distribution functions were determined from birefringence data for each CNC as follows;

1) C-CNC

$$v = (1.80 \times 10^{19}) \times \sum_{i=1}^{10} \left(\frac{L_i}{40}\right)^3 \exp\left(-\frac{L_i}{40}\right) \quad (\text{S8})$$

where

$$L_i = 25(2i - 1) \quad (\text{S9})$$

2) S-CNC

$$v = (4.10 \times 10^{18}) \times \sum_{i=1}^{13} \left(\frac{L_i}{45}\right)^3 \exp\left(-\frac{L_i}{45}\right) \quad (\text{S10})$$

where

$$L_i = 25(2i - 1) \quad (\text{S11})$$

3) T-CNC

$$v = (2.42 \times 10^{17}) \times \sum_{i=1}^{14} \left(\frac{L_i}{220}\right)^3 \exp\left(-\frac{L_i}{220}\right) \quad (\text{S12})$$

where

$$L_i = 100(2i - 1) \quad (\text{S13})$$

The number of classes and class values L_i were determined according to the length distribution histograms determined by TEM (Figure 1d–1f).

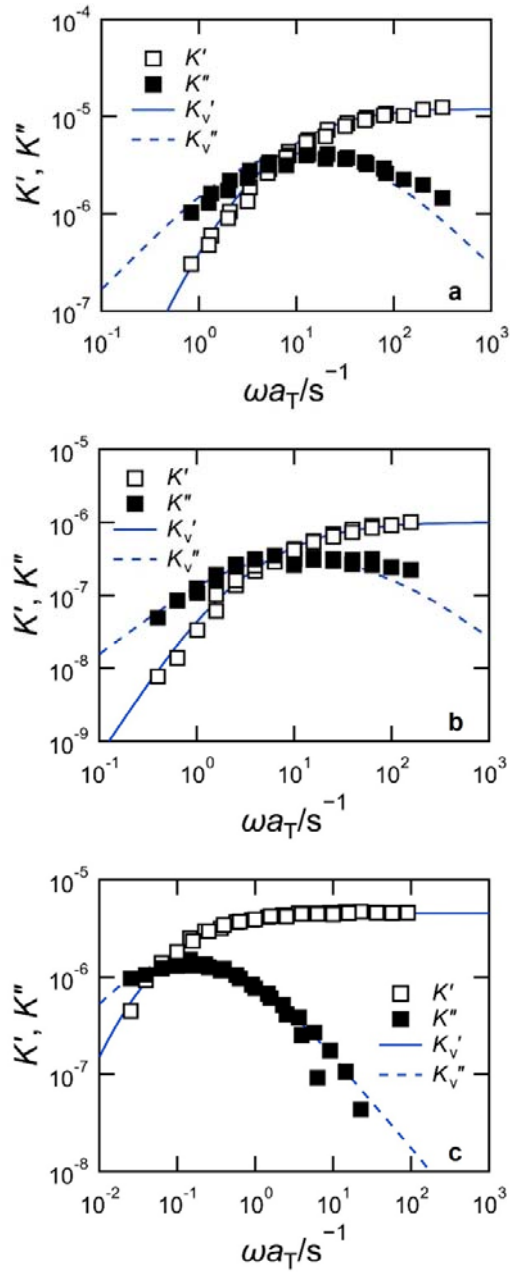


Figure S3. Comparison of the experimental K' and K'' values for the 0.15% w/w C-CNC/glycerol (a), 0.01% S-CNC/glycerol (b), and 0.03% T-CNC/glycerol dispersions with the K_v' and K_v'' values calculated using Eqns 5 and 6, respectively.

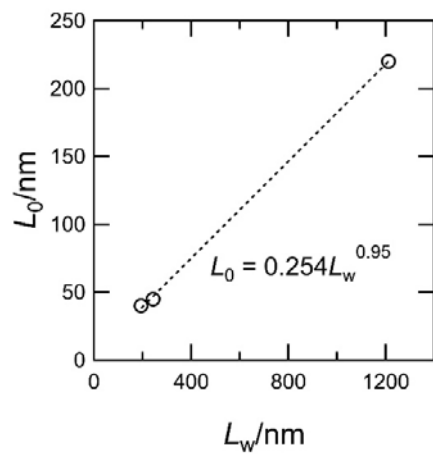


Figure S4. Fitting parameter L_0 of the length distribution functions determined from the birefringence data as a function of length-weighted mean length L_w .

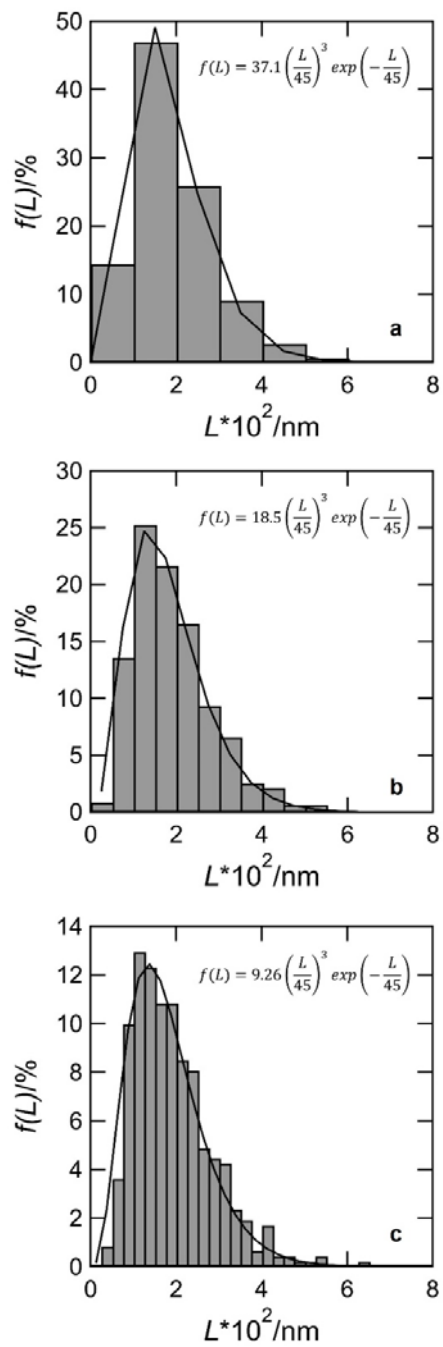


Figure S5. The influences of class divisions of length distributions on the length distribution functions Eq. 7: (a) course- and (c) fine-divided length distributions. The data of the S-CNC shown in Figure 5b was used as a standard (b).

S5. Comparison of viscoelastic data with the theory for the viscoelasticity of rigid rods in the dilute regime

The experimental G' and G'' values were compared with the theory for the viscoelasticity of rigid rods in the dilute regime. When a dilute dispersion of rigid rods is subjected to steady shear flow, rigid rods are oriented by the flow. As a result, entropy decrease, and then stress occur. The rate of which the orientation reverts to random orientation is characterized by the relaxation time τ_{rod} . Based on the theory which describes the orientation of rigid rods,⁹ the storage modulus G_{rod}' and loss modulus G_{rod}'' for rigid rods are given by

$$G_{rod}' = \frac{3}{5} \nu k_B T \omega^2 \tau_{rod}^2 / (1 + \omega^2 \tau_{rod}^2) \quad (S14)$$

$$G_{rod}'' = \nu k_B T \omega \tau_{rod} \left[\frac{3}{5} / (1 + \omega^2 \tau_{rod}^2) + A \right] \quad (S15)$$

where ν is the number of CNCs per unit volume, k_B is the Boltzmann constant, T is the temperature, and A is a numerical coefficient depending on the aspect ratio. In the present study, A was substituted with 0.29, as was reported by Yamakawa et al.¹⁰ The relaxation time for rotational motions of rigid rods τ_{rod} is given by³

$$\tau_{rod} = \frac{1}{6D_r} = \pi \eta_s L^3 / \{18k_B T [\ln(L/d) - 0.8]\} \quad (S16)$$

where D_r is the rotational diffusion coefficient, η_s is the dispersion medium viscosity, L is the CNC length. Diameter d was substituted with the square root of the product of W_w and h (Table 1). To take the length distribution into account, the $G_{rod}'(L)$ and $G_{rod}''(L)$ were first calculated using the class value as L for each class of the TEM-determined

length distribution histograms, and then added together. The obtained values were used for the comparison with the experimental values. The experimental G' and G'' values of the C-CNC were in good agreement with their G_{rod}' and G_{rod}'' values, respectively, at frequencies lower than 100 s^{-1} (Figure S6a). That is, the relaxation derived from the rotation of rods was measured. The experimental G' and G'' values at high frequencies ($> 100 \text{ s}^{-1}$) were unmeasurable because of the low viscosity of the C-CNC/glycerol dispersion. The experimental G' values of the S-CNC and T-CNC departed from the G_{rod}' values with increasing the frequencies at high frequencies ($> 10 \text{ s}^{-1}$) (Figure S6b and S6c). The viscoelastic data of S-CNC and T-CNC was not fitted by the theory for viscoelasticity of rigid rods in dilute regime at high frequencies (Figure S6b and S6c).

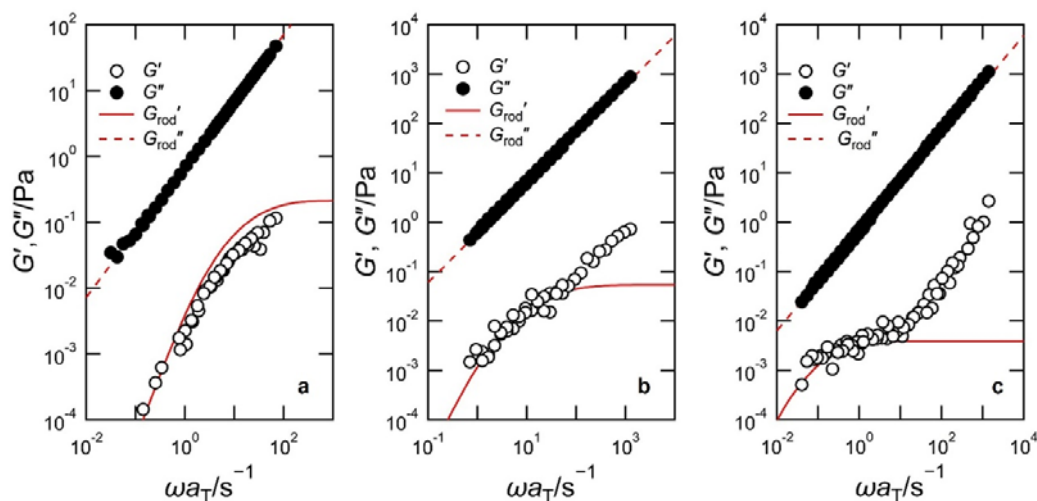


Figure S6. Comparison of experimental G' and G'' values for the (a) 0.15% w/w C-CNC, (b) 0.01% w/w S-CNC, and (c) 0.03% w/w T-CNC/glycerol dispersions with their theoretical G_{rod}' and G_{rod}'' values calculated using Eqns S14 and S15.

References

1. Itou, T.; Chikiri, H.; Teramoto, A.; Aharoni, S. M., Wormlike Chain Parameters of Poly(hexyl isocyanate) in Dilute Solution. *Polym. J. (Tokyo, Jpn.)* **1988**, *20*, 143–151.
2. Kasabo, F.; Kanematsu, T.; Nakagawa, T.; Sato, T.; Teramoto, A., Solution Properties of Cellulose Tris(phenyl carbamate). 1. Characterization of the Conformation and Intermolecular Interaction. *Macromolecules* **2000**, *33*, 2748–2756.
3. Doi, M.; Edwards, S. F., In *The Theory of Polymer Dynamics*. Oxford University Press Inc.: New York, NY, 1986; p 312.
4. Shankar, V.; Pasquali, M.; Morse, D. C., Theory of Linear Viscoelasticity of Semiflexible Rods in Dilute Solution. *J. Rheol.* **2002**, *46*, 1111–1154.
5. Okada, Y.; Goto, Y.; Tanaka, R.; Katashima, T.; Jiang, X.; Terao, K.; Sato, T.; Inoue, T., Viscoelastic Properties of Tightly Entangled Semiflexible Polymer Solutions. *Macromolecules* **2018**, *51*, 9626–9634.
6. Janeschitz-Kriegl, H., In *Polymer Melt Rheology and Flow Birefringence.*, 1st ed.; Springer-Verlag Berlin Heidelberg: New York, NY, 1983; p 60–66
7. Tanaka, R.; Kuribayashi, T.; Ogawa, Y.; Saito, T.; Isogai, A.; Nishiyama, Y., Ensemble Evaluation of Polydisperse Nanocellulose Dimensions: Rheology, Electron microscopy, X-Ray Scattering and Turbidimetry. *Cellulose* **2017**, *24*, 3231–3242.
8. Lake, J., An Iterative Method of Slit-Correcting Small Angle X-Ray Data. *Acta crystallogr.* **1967**, *23*, 191–194.
9. Ferry, J. D., In *Viscoelastic Properties of Polymers*, 3rd ed.; John Wiley & Sons: New York, NY, 1980; p 179.
10. Yamakawa, H., Viscoelastic Properties of Straight Cylindrical Macromolecules in Dilute Solution. *Macromolecules* **1975**, *8*, 339–342.